Effect of δ Alumina Fibers on the Aging Characteristics of 2024-Based Metal-Matrix Composites

KUO-CHAN CHEN and CHUEN-GUANG CHAO

The age-hardening precipitation reaction in aluminum matrix composites reinforced with discontinuous alumina fibers was studied using the differential scanning calorimetry (DSC) technique, microhardness tests, and transmission electron microscopy (TEM) observation. Composites fabricated with the 2024 alloy matrix were infiltrated through a ceramic preform using a squeeze-casting process. The alumina fibers had a considerable effect on the aging response of the matrix alloy in composites. Alumina fibers caused suppression of Guinier–Preston (GP) zone formation in composite that reduced the peak hardening during artificial aging. The suppression of GP zone formation in composites is believed to be due to the fiber-matrix interface, which acts as a sink for vacancies during quenching. Moreover, the presence of reinforcement does not alter the kinetics of the subsequent artificial aging of these Al_2O_3/2024Al composites.

I. INTRODUCTION

METAL-matrix composites (MMCs) have been the object of intense research for many years. Fiber-reinforced MMCs offer many advantages in applications where low density, high strength, and high stiffness are of prime concern. Most of the alloys that were employed as matrices in MMCs are light alloys, particularly those based on aluminum. These matrix alloys have included both non-heat-treatable and heat-treatable alloys. The heat-treatable alloys such as 2xxx, 6xxx, and 7xxx constitute a metallurgically "active" component of the MMC whose properties can be deliberately altered to influence the properties of the final composite. However, designing the composite microstructure and aging treatments, so that they are based directly on the precipitation characteristics of the unreinforced matrix material, may impair strengthening without fully utilizing the potentiality of the composite material. It was observed that the aging kinetics are enhanced or retarded by reinforcing the matrix alloy during a heat treatment in different MMC materials. An accelerated aging phenomenon was reported in the 6061Al-B_4C particulates composite,[1] the 2024Al-SiC whisker composite,[2] and the Al-Si-Mg/SiC composites.[3] The authors attributed this acceleration to the presence of high diffusivity paths in the composite, particularly the reinforcement-matrix interfaces and the dislocations introduced by differential thermal expansion. On the contrary, Ceresara and Fiorini reported that the suppression of the Guinier–Preston (GP) zone formation was observed in sintered aluminum powder (SAP) type Al-Cu/Al_2O_3[4] and Al-Mg-Si/Al_2O_3.[5] The most probable reason of such a phenomenon was suggested to be the lack of quenched-in vacancies following the solution treatment, due to the availability of a large number of vacancy sinks at reinforcement-matrix interfaces.

Dutta et al.[6] reported that the aging kinetics in cast materials are considerably slower than those in powder metallurgy (PM) processed materials. Nutt and Carpenter[7] reported the interfacial segregation of magnesium and the heterogeneous distribution of matrix phase in the SiC whisker-reinforced 2024Al alloy. Friend and Luxton[8] indicated that the fiber array has a considerable effect on the age-hardening response of the matrix alloy in MMCs, causing suppression of GP zone formation, which inhibits natural and artificial aging. Obviously, the aging characteristics depended on the following: reinforcement, alloy composition, heat treatment, processing method, and processing parameters. The purpose of this article is to document the effect of alumina fiber reinforcement on the aging response of a cast 2024Al matrix composite. The aging behavior of 2024Al/Al_2O_3 composites was studied using the differential scanning calorimetry (DSC) technique, microhardness tests, and transmission electron microscopy (TEM) observations.

II. EXPERIMENTAL PROCEDURE

The base matrix was a heat-treatable 2024Al of which compositions are given in Table I. The composite materials were produced by squeeze casting. SAFFIL* Al_2O_3

---

*SAFFIL is a trademark of ICI Americas, Inc., Wilmington, DE.

---

short fibers (3 μm in diameter) were fabricated into a 20 × 18 × 100 mm preform block by press forming. Figure 1 shows a schematic diagram of preform fabrication. In this case, short fibers were mixed homogeneously with water, accompanied by a small addition of binder (SiO_2 nH_2O). During press forming, the slurry was poured into the mold, and dewatering was conducted while the final preform was shaped. The fiber volume fraction of the composites was 9 and 14 pct. The apparatus used for the fabrication of the composite material is shown in Figure 2. The preform was preheated to 800 °C and introduced to the mold, which was preheated to 300 °C. The liquid aluminum alloy, at 800 °C,

KUO-CHAN CHEN, Graduate Student, and CHUEN-GUANG CHAO, Associate Professor, are with the Institute of Materials Science and Engineering, National Chaio Tung University, Hsinchu, Taiwan 30049, Republic of China.
Manuscript submitted February 7, 1994.

Table I. Composition of 2024 Alloy (Weight Percent)

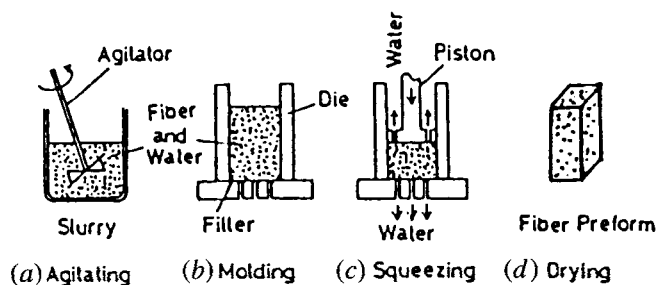| Cu	Mg	Mn	Fe	Si	Al
4.26	1.16	0.50	0.11	0.08	balance

Fig. 1—Fabrication processes of a short-fiber preform, showing the press forming.
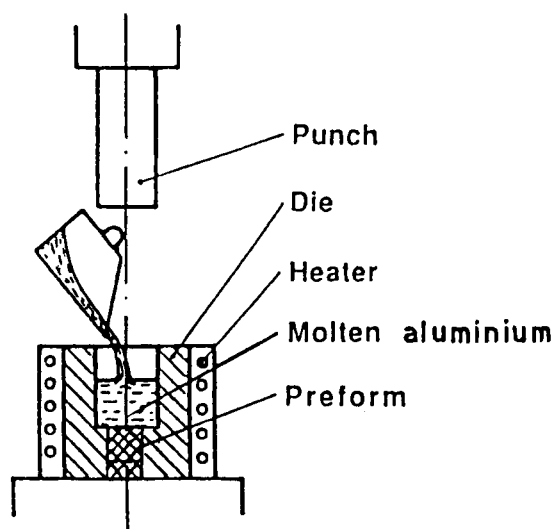

Fig. 2—Schematic illustration of the squeeze casting apparatus.

was squeezed into a fiber preform by a 50 MPa hydraulic press to form the composites. The pressure holding time was 65 seconds. Microstructural characterization was carried out by using optical microscopy. The as-cast specimens were cut from a 5.5-mm-diameter cylindrical block. Specimens were solution treated at 500 °C for 3, 24, 72, and 120 hours. Then, specimens were quenched into water or ice brine (−17 °C). Aging was carried out in an oil bath at 190 °C for 1, 4, 8, 12, and 24 hours.

All the treated specimens were immediately stored in a −15 °C refrigerator. Discs (5.5-mm diameter and 0.4-mm thickness) for DSC were polished and weighed. The DSC analysis was performed by using a Du Pont 2910 thermal analyzer. Disc samples were loaded in a DSC cell at room temperature and equilibrated for a few minutes. The heating rate was 10 °C/min from 30 °C to 550 °C. Dry nitrogen was purged through the cell at the rate of 40 mL/min to avoid oxidation. Output for all DSC runs was recorded in the instrument memory. At least three samples were measured for each heat treatment. In order to evaluate the peak area of the DSC curve,

the DSC scan of a sample was interrupted just as the S' formation reaction was finishing, and the scan was run again as a baseline. Vickers hardness measurement on the matrix (between fibers) of heat-treated specimens was made using a diamond pyramid indenter and 50-g load. At least 10 hardness measurements were made for each aging condition to ensure accurate results. The TEM specimens of the unreinforced alloy were prepared by means of a double-jet electropolisher. However, this was impossible for the composites because of differential electropolishing effects. The TEM specimens of composites were prepared by ion thinning at an accelerating voltage of 5 KV and 13 deg with a liquid nitrogen cold stage after using dimpler to ground to a 10-μm thickness. Transmission electron microscopy was performed on JEOL* 2000FX scanning transmission electron

---

*JEOL is a trademark of Japan Electronic Optics Ltd., Tokyo, Japan.

---

microscope operated at 160 KV.

III. RESULTS

A. Microstructure

Figure 3(a) shows an etched optical micrograph of the 2024Al alloys. Figures 3(b) and (c) show etched optical micrographs of the nominally 9 and 14 pct Vf composite in the cast condition. All materials have segregation in dendritic interstices. The dendrite arm spacing of composites (about 15 μm) is smaller than that of 2024Al (about 25 μm). It is suggested that Al_2O_3 fibers act as obstacles during solidification. Figure 4 shows typical micrographs of solution-treatment materials. The segregation and dendrite structure are eliminated by solution treatment.

B. DSC

1. Solution treatment

For comparison purposes, results from DSC scans of the 2024Al, 9 pct Al_2O_3/2024Al and 14 pct Al_2O_3/2024Al composites quenched into water are shown in Figure 5. The curve from 2024Al shows four zones: exothermic between 40 °C and 142 °C due to the formation of GP zones; endothermic between 140 °C and 255 °C due to the dissolution of GP zones; exothermic between 255 °C and 355 °C due to the formation of S' precipitate; and endothermic between 355 °C and 500 °C due to the dissolution of S' precipitate. This result is similar to 2124Al reported by Papazian.[9] However, curves of both 9 pct Al_2O_3 and 14 pct Al_2O_3 composites do not have obvious GP zone formation and dissolution peaks. Curves in Figure 6 show the same precipitate reactions after ice brine quenching (−17 °C). All the curves have an obvious GP zone formation and dissolution peaks.

2. Isothermal artificial aging

The results (Figure 7) of DSC measurements on 2024Al quenched from 500 °C into water and artificially aged at 190 °C for various aging periods (1, 4, 8, 12, and 24 hours) indicate that the S'-phase formation peak becomes progressively less prominent with increase in aging time. The values of enthalpy of S'-phase formation are listed in Table II. The peak finally almost disappears after
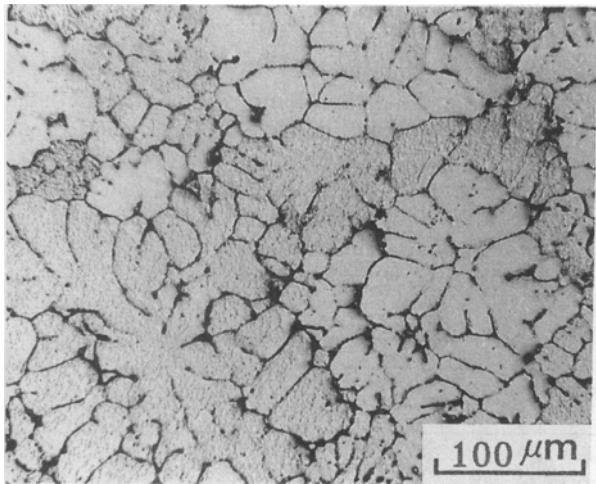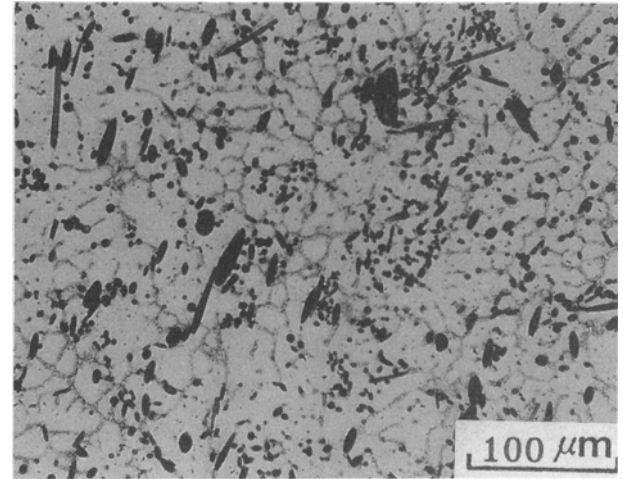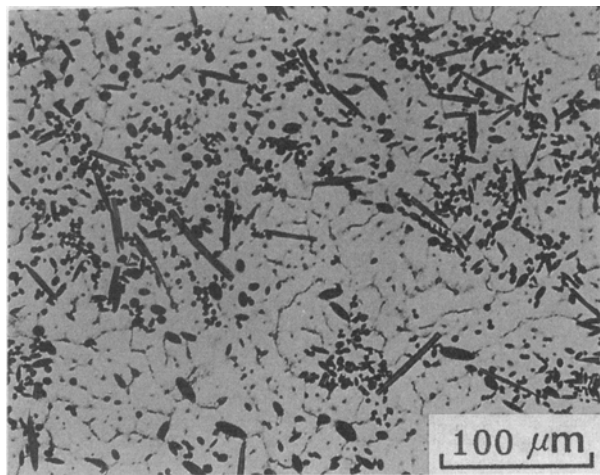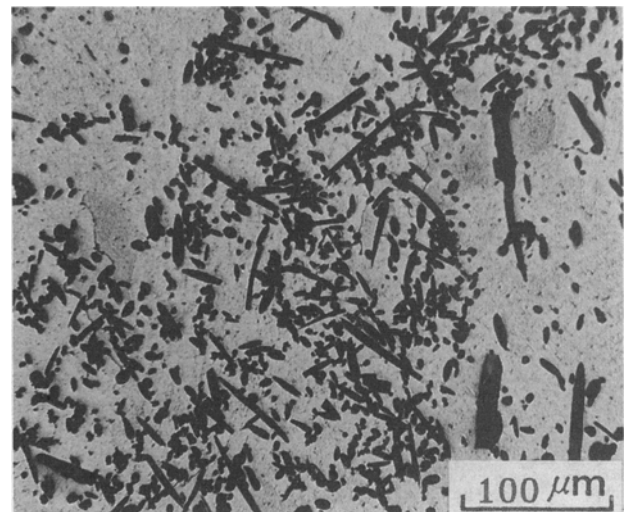
(a)
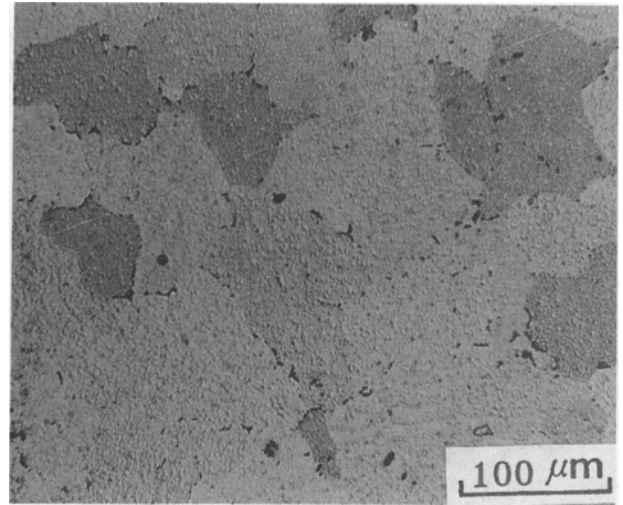
(a)
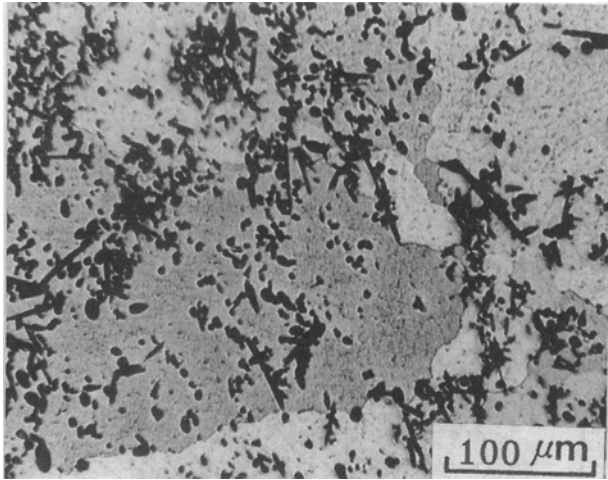
(b)

(b)

(c)

(c)

Fig. 3—Etched optical micrographs of the as-cast materials: (a) 2024Al, (b) 9 pct Al$_2$O$_3$ composite, and (c) 14 pct Al$_2$O$_3$ composite.

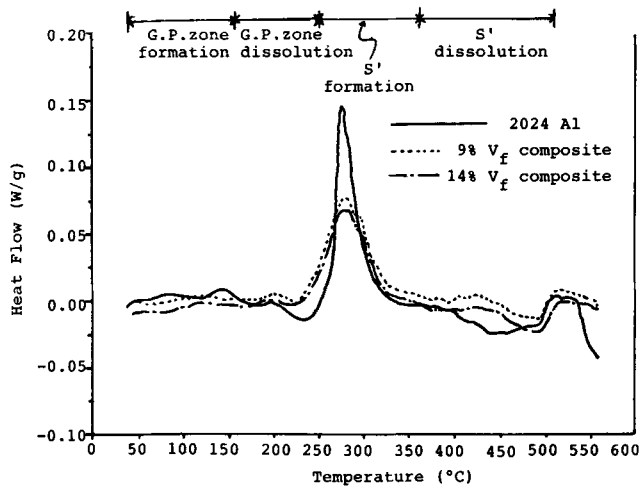Fig. 4—Etched optical micrographs of solution-treated materials: (a) 2024Al, (b) 9 pct Al$_2$O$_3$ composite, and (c) 14 pct Al$_2$O$_3$ composite.

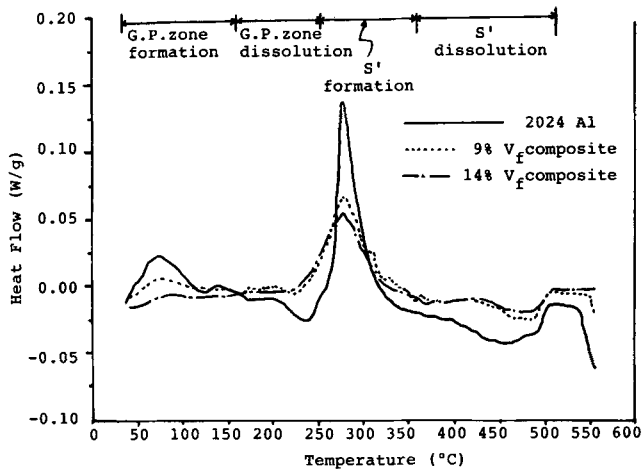Fig. 5 — Results of the DSC for the solution-treated and water-quenched materials.

aging for 24 hours. However, a similar trend was found in Figures 8 and 9 for both 9 and 14 vol pct composites, respectively, after aging for only 8 hours.

3. Matrix microhardness

Generally speaking, the composite hardness contains contributions from both the metallurgically active matrix and the fiber. When the composite is cooled from elevated temperature of aging process, misfit strains occur due to differential thermal contraction at the reinforcement/matrix interface, which are sufficient to

Table II. Enthalpy of S'-Phase Formation (J/g)

Aged Time (h)	0	1	4	8	12	24
2024Al	23.8	20.4	16.8	10.6	9.2	3.56
9 pct Vf^*	22.8	16.6	5.9	1.9	0.7	—
14 pct Vf^*	21.7	17.2	4.9	1.4	0.3	—

*Composite.

Fig. 6 — Results of the DSC for the solution-treated and ice-brine-quenched (-17 °C) materials.

Fig. 8 — Results of the DSC for 9 pct Al_2O_3 composites, artificially aged at 190 °C: (a) as-quenched, (b) aged for 1 h, (c) aged for 4 h, (d) aged for 8 h, (e) aged for 12 h, and (f) aged for 24 h.
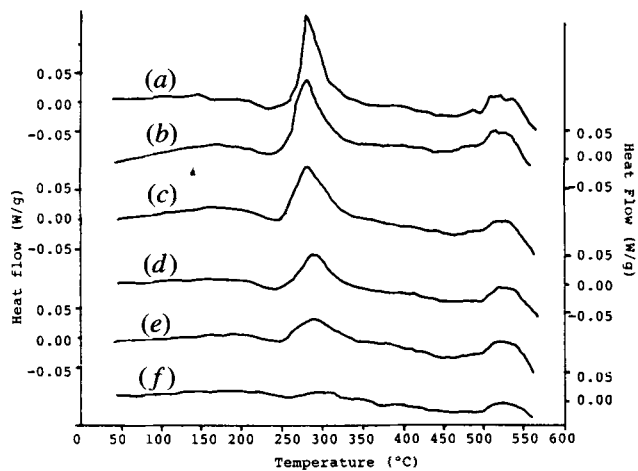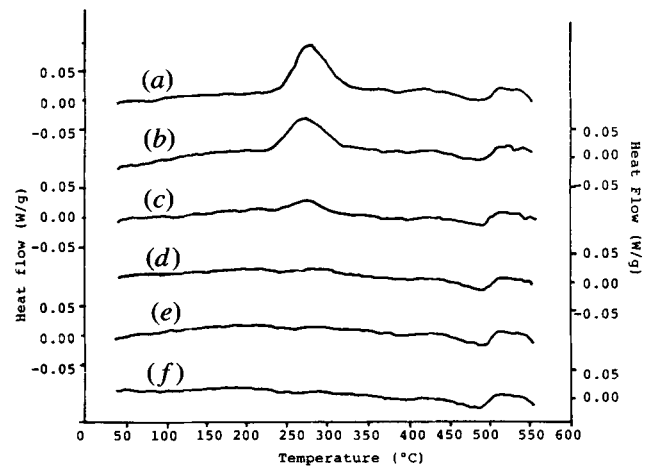

Fig. 7 — Results of the DSC for unreinforced 2024Al, artificially aged at 190 °C: (a) as-quenched, (b) aged for 1 h, (c) aged for 4 h, (d) aged for 8 h, (e) aged for 12 h, and (f) aged for 24 h.

Fig. 9 — Results of the DSC for 14 pct Al_2O_3 composites, artificially aged at 190 °C: (a) as-quenched, (b) aged for 1 h, (c) aged for 4 h, (d) aged for 8 h, (e) aged for 12 h, and (f) aged for 24 h.
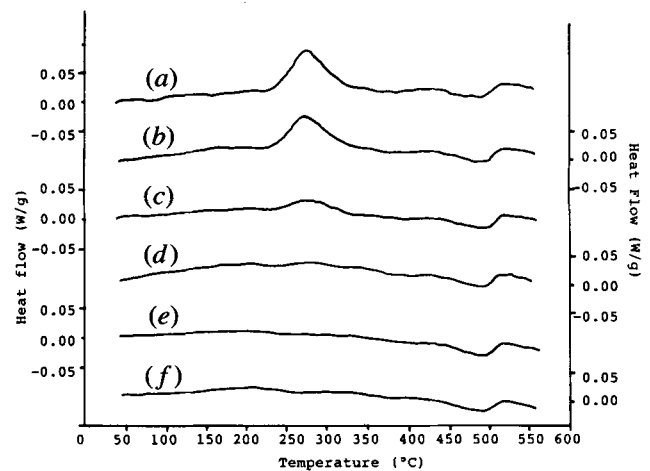
generate dislocations. The dislocation density is able to influence the microhardness. However, in our TEM observations, the dislocation density of composites is very low. The results are different with the Al/SiC composite that had a high dislocation density in the Al matrix for 12 hours at 810 K.[10] The coefficient of thermal expansion (CTE) difference between Al and SiC is 10:1[10,11] and that between Al and Al$_2$O$_3$ is 3:1. Low dislocation density in our present study results from thermal stress in Al/Al$_2$O$_3$ to be insufficient to generate a large amount of dislocations in the matrix of composites. We can neglect the influence of dislocation density generated by thermal stresses on microhardness. However, it is assumed that the age-hardening treatment only affects the matrix properties. According to this investigation, the microhardness of matrix in composite displays the effect of reinforcement on the aging characteristic of composite. Figure 10 shows the microhardness change of the 2024Al alloy and composites during isothermal aging at 190 °C. The microhardness of the matrix at peak hardness (aged 8 hours at 190 °C) decreases with increasing volume fraction of fiber reinforcement. The microhardness of 2024Al is higher than that of composites.

4. TEM observation

Both unreinforced 2024Al alloy and Al$_2$O$_3$/2024Al composites are observed in a rodlike undissolved phase after a 24-hour solution treatment. In order to clarify the undissolved phase, a scanning transmission electron microscopy–energy-dispersive spectroscopy (STEM-EDS) study was undertaken. Figure 11(a) shows a typical EDS spectrum taken from the rodlike undissolved phase, where copper, magnesium, aluminum, manganese, and iron peaks were examined. The average elemental distributions of metal atoms in this phase were listed in Figure 11(b). It is clearly seen that the content of copper and manganese of the undissolved phase are much higher than that of the matrix. Figures 12(a) and (b) are bright-field (BF) electron micrographs showing the rodlike phase in both 2024Al and Al$_2$O$_3$/2024Al composites, respectively. Figure 12(c) shows the diffraction pattern from the matrix and the undissolved phase. The relationship obtained from the analysis is $(100)\alpha//(100)_u$, $(010)\alpha//(010)_u$. The undissolved phase was identified as a

Cu$_2$Mn$_3$Al$_{20}$ phase, which was found in 2014Al by Christman and Suresh.[2]

Figure 13(a) shows the BF electron micrograph of 2024Al aging at 190 °C for 24 hours. The matrix microstructure consists of S'(Al$_2$CuMg) precipitates appearing as needles or laths. Figures 13(b) and (c) indicate that the selected area diffraction pattern (SADP) of S' phase with zone axis is [100] and [012]. The S' phase obviously has a $[100]\alpha//[010]_{S_{a'}}$; $[001]\alpha//[012]_{S_{a'}}$ orientation relationship.

Microstructural development of the unreinforced 2024Al alloy and Al$_2$O$_3$/2024Al composites in response to aging treatment at 190 °C is shown in Figures 14 and 15, respectively. The TEM results indicate the early stages of S' precipitate of 2024Al on dislocation loops (4 hours aging time) shown in Figures 14(a) and (b). Figures 14(c) and (d) show that the micrographs after 8 and 12 hours of aging time have needle precipitates. The progressive development of S' precipitate in composites is similar with unreinforced 2024Al expect the slightly difference of precipitate size, as shown in Figure 15. The S' precipitate of 2024Al keeps continuous growth after aging for 12 hours, while the S' precipitate of composites is almost the same size after aging for 8 hours. The probable reason is that the magnesium content is exhausted after aging for 8 hours in composites due to the occurrence of spinel (MgAl$_2$O$_4$) in the interface of Al$_2$O$_3$/Al-Mg-Cu composites.[12] The undissolved phase can also influence the aging process. Figure 16 shows that a precipitate-free zone appears near the undissolved phase (Cu$_2$Mn$_3$Al$_{20}$). This is because a depletion zone of copper near the undissolved phase causes the S' precipitate-free zone.
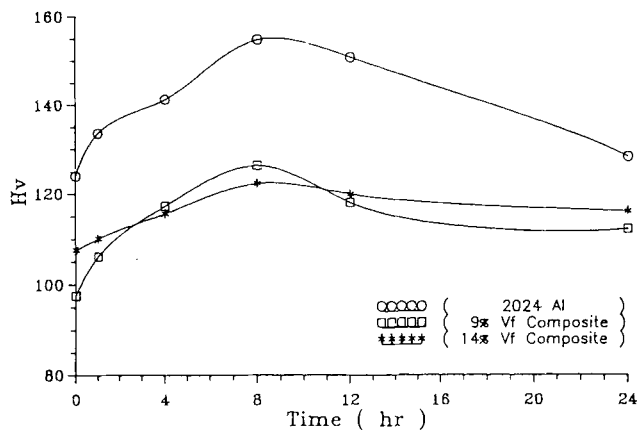

Fig. 10—Microhardness as a function of aging time at 190 °C for the unreinforced 2024Al and composite with 9 and 14 vol pct Al$_2$O$_3$.

(a)

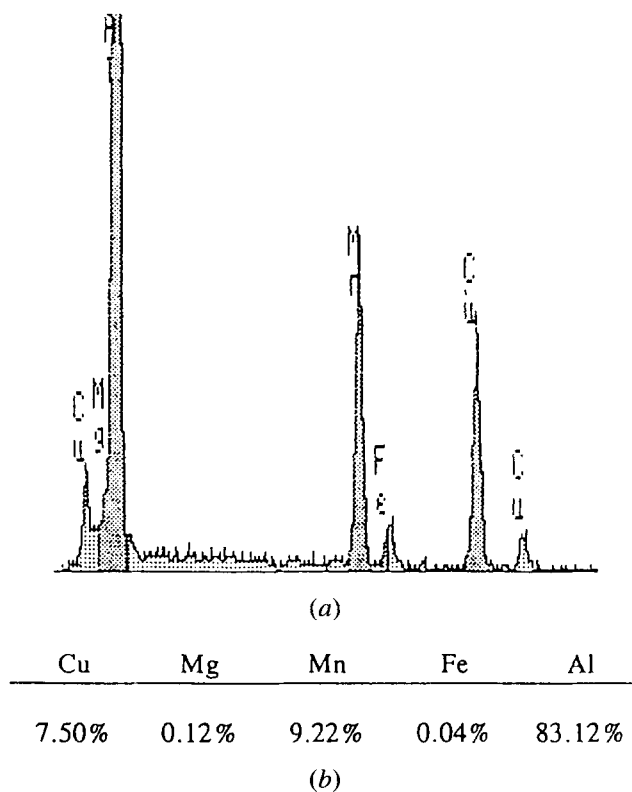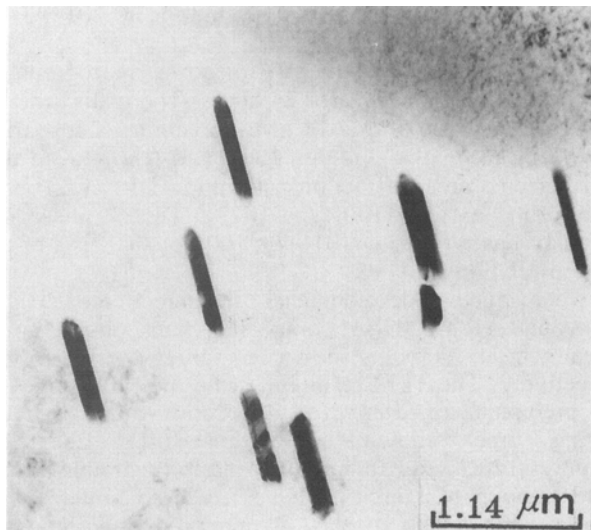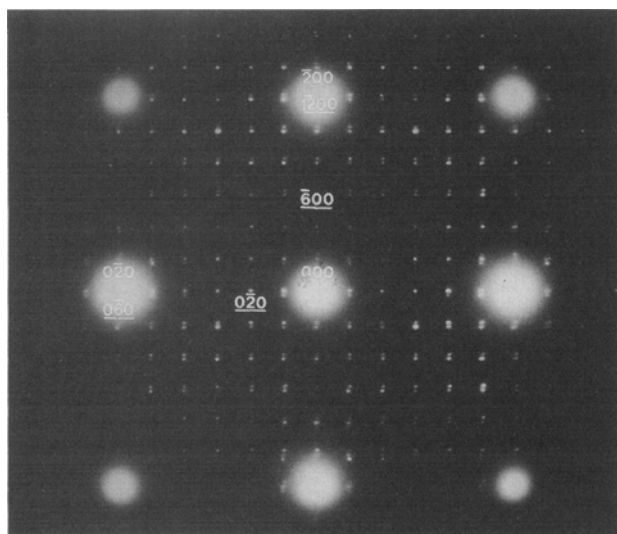| Cu	Mg	Mn	Fe	Al
7.50%	0.12%	9.22%	0.04%	83.12%

(b)

Fig. 11—(a) An EDS spectrum taken from the rodlike undissolved phase and (b) the average elemental distributions of metal atoms.
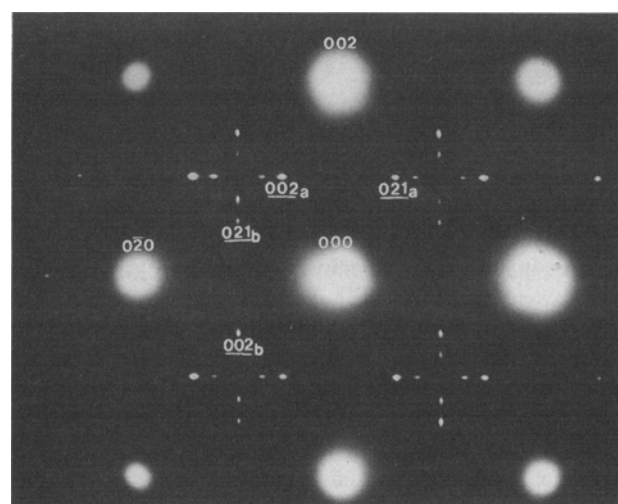
(a)

(a)

(b)

(b)

Fig. 12 — (a) The BF electron micrographs of the undissolved phase in 2024Al; (b) 9 pct Vf composite and z = [001] diffraction pattern (hkl = a phase, $\underline{hkl}$ = undissolved phase).

IV. DISCUSSION

The area of the peak in the DSC curve gives the reaction enthalpy that is directly related to the molar heat of reaction and the volume fraction of the precipitating or dissolving phase,[13] while the temperature is related to the size and stability of the precipitate and to the reaction kinetics.[14,15] The curves in Figure 6 show that the enthalpy of GP zone formation is significantly different. It decreases with increasing volume fraction of fiber; i.e., the volume fraction of the GP zone is decreasing with increasing Al_2O_3 reinforcement. The enthalpy value of GP zone formation is listed in Table III. It is clear that GP zone formation is inhibited in the composites. This inhibition of GP zone formation and its effect of age hardening are similar to the observation in the SAP[4,5] alloy. In SAP alloys, these phenomena have
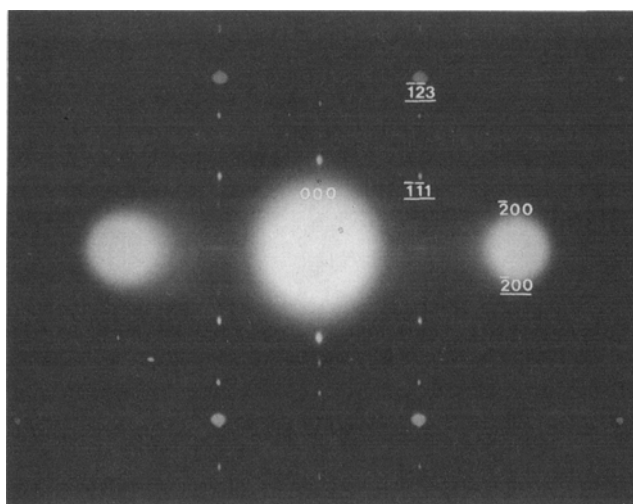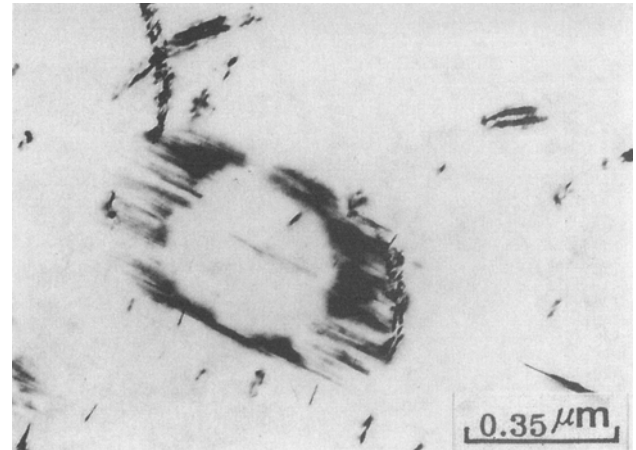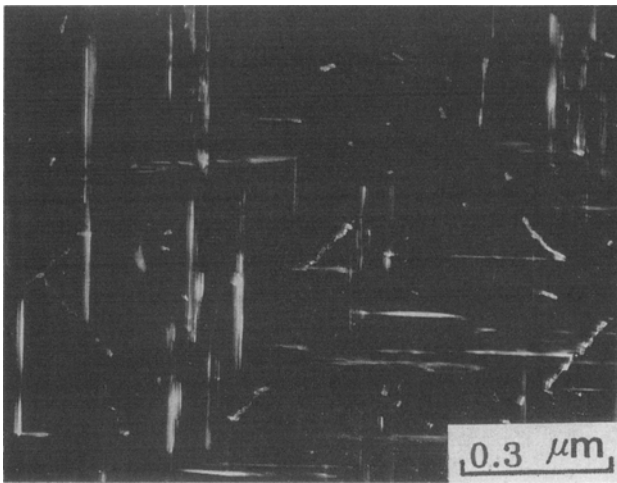

(c)

Fig. 13 — (a) BF micrographs of 2024Al aging at 190 °C for 24 h, showing S' precipitate in matrix; (b) SADP showing B = [100]; and (c) SADP showing B = [012] (hkl = a phase, $\underline{hkl}$ = phase).
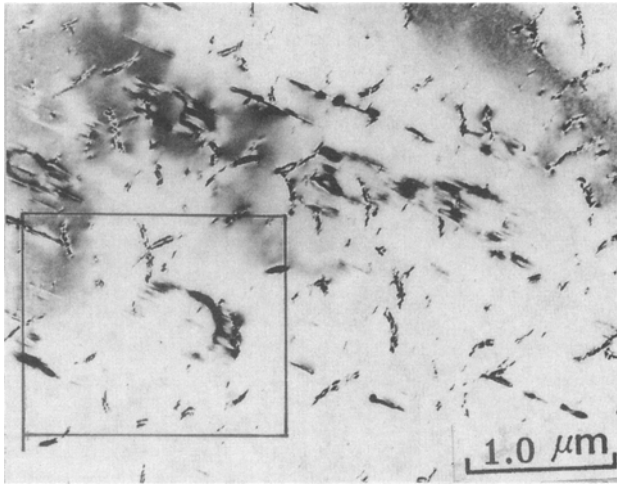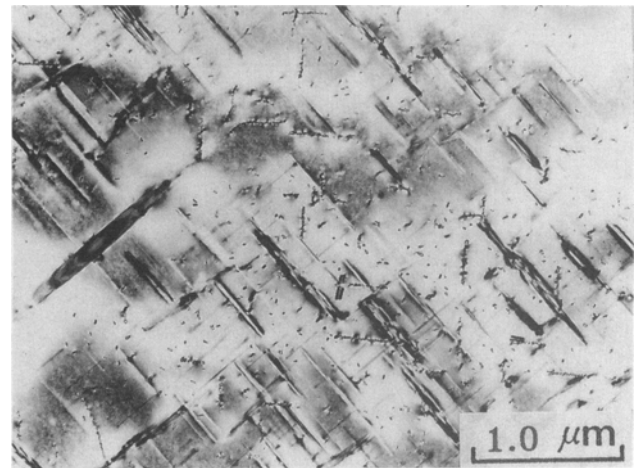
(a)

(b)

(c)

(d)

Fig. 14—Microstructural development of the unreinforced 2024Al in response to aging treatment at 190 °C for (a) 4 h, (b) enlargement of (a), (c) 8 h, and (d) 12 h.

been attributed to a lack of quenched-in vacancies that were soaked up by the grain boundaries in the fine-grain matrix and by the Al/Al$_2$O$_3$-particle interface. The observations in the present work suggest that a similar mechanism is responsible for the inhibition of GP zone formation in MMC matrices. There is no significant difference between the grain size of the unreinforced alloy and composites. It implies a constant grain-boundary "vacancy-sink" potential for both the alloy and composites. Thus, the fiber-matrix interfaces must play the predominant role as vacancy sinks. This is consistent with GP zone suppression dependence of the fiber volume fraction. The quenched-in vacancies can much slower diffuse to sinks at fiber-matrix interface during the quenching into ice brine (−17 °C); i.e., the quenched-in vacancy concentration after ice brine quenching is higher than that after water quenching. This exhibits that the formation of the GP zone relies on the presence of quenched-in vacancies to aid the diffusion of the element atoms. Therefore, Figure 6 shows that the GP zone formation obviously increases.

In the as-quenched condition, the composite, either 9 pct V_f or 14 pct V_f, has a hardness less than that of the unreinforced matrix. The result is similar to the 2124Al-SiC composites reported by Christman and Suresh.[2] It had taken 4 to 5 hours to prepare the microhardness specimen at as-quenched condition. The natural aging is suggested to lead to the higher microhardness of 2024Al. The total amount of S' precipitation decreases with increasing fiber volume fraction according to the results of Table II. Since the natural or artificial age hardening of 2024Al is attributed to the GP zone and the S' phase, the microhardness of composites is smaller due to the suppression of the GP zone and the S' formation in matrix of composites. These can explain that the microhardness of 2024Al is higher than that of composites shown in Figure 8. In the meantime, the lack of GP zones not only inhibits natural aging but also has a considerable effect on the later stages of age hardening. The suppression of GP zone formation during the early stage of artificial aging means that no nuclei are produced for S' formation until a considerably later stage of
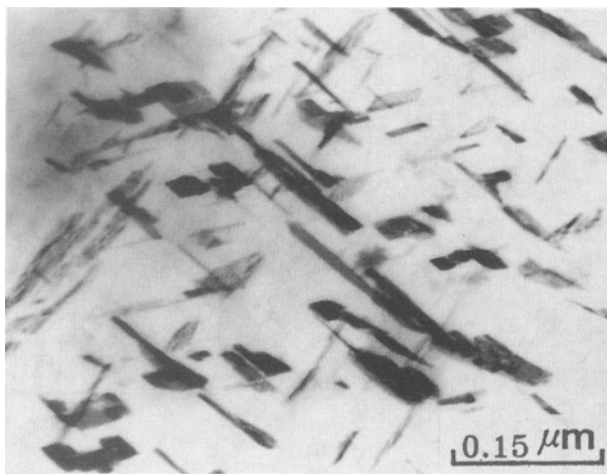
(a)
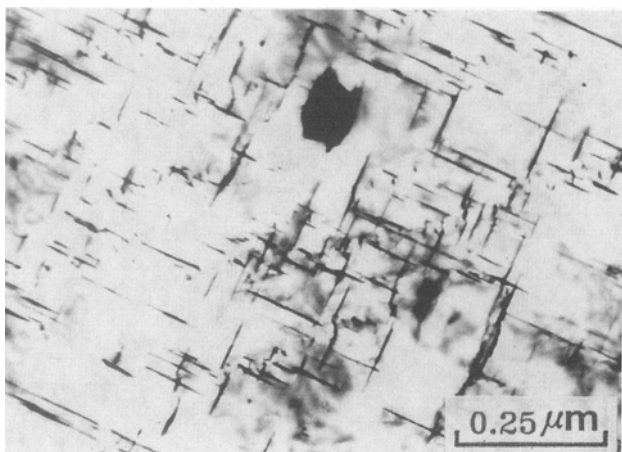
(b)
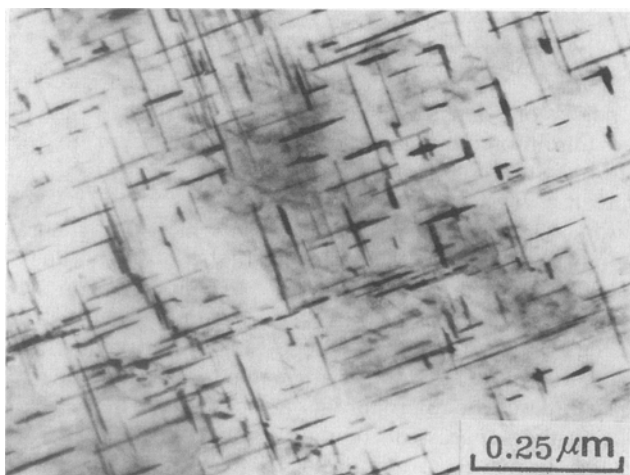
(c)

Fig. 15 — Microstructural development of the composites in response to aging treatment at 190 °C for (a) 4 h, (b) 8 h, and (c) 24 h.
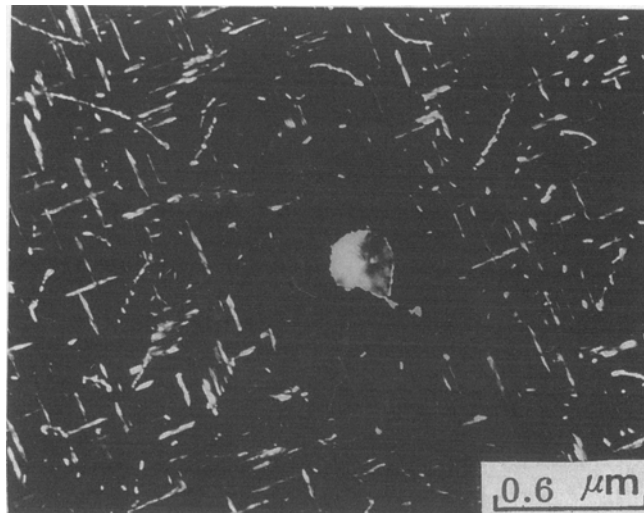

Fig. 16 — TEM micrograph of the aged 2024Al at 190 °C for 12 h, showing a precipitate-free zone near the undissolved phase.

Table III. Enthalpy of GP Zone Formation (J/g)

2024Al	9 Pct Vf Composite	14 Pct Vf Composite
7.4	2.6	2.1

the aging process; it matches the results of Table II. The enthalpies of S' formation listed in Table II indicate the residual amount of S' phase after various aged times. The fact that the enthalpy of S' formation of composites rapidly decreases at 4 hours of aging means that few nuclei are produced for S' formation until considerably later stages (4 hours) of the aging process. Note also that the degree of hardening due to aging is not reduced in the case of the 9 pct Vf but reduced by ~50 pct in the case of 14 pct Vf. However, the reason is still not yet clear. Moreover, the S'-phase formation peak of 2024Al and composites is at the same temperature (277 °C); *i.e.*, the maximum reaction rate of the S' precipitate is at the same temperature. In other words, the presence of reinforcement does not alter the kinetics of aging in $Al_2O_3/$2024Al composites.

V. CONCLUSIONS

In our present study, the effect of reinforcement on the aging characteristics of cast $Al_2O_3/$2024Al composites is summarized in the following:

1. The suppression of GP zone formation in composites is observed since the fiber-matrix interface acts as a sink for vacancies during quenching.
2. The S' precipitate reaction aged at 190 °C is finished earlier in composites because the total amount of S' precipitate in the composites is less than that in unreinforced 2024Al.
3. The microhardness value of the peak of the matrix in composites is lower than that of 2024Al. The reason is believed to be due to the suppression of GP zone and S'-phase formation in the matrix of composites.

4. Both the unreinforced 2024Al and composite materials occur in the S'-phase formation peak at the same temperature (277 °C). This means that the presence of reinforcement does not alter the kinetics of aging in composites.

REFERENCES

1. T.G. Nich and R.F. Karlak: *Scripta Metall.*, 1984, vol. 18, pp. 25-28.
2. T. Christman and S. Suresh: *Acta Metall.*, 1988, vol. 36 (7), pp. 1691-704.
3. J.P. Cottu, J.J. Couderc, B. Vignier, and L. Bernard: *J. Mater. Sci.*, 1992, vol. 27, pp. 3068-74.
4. S. Ceresara and P. Fiorini: *Powder Metall.*, 1981, No. 4, pp. 210-13.
5. S. Ceresara and P. Fiorini: *Powder Metall.*, 1979, No. 1, pp. 1-4.
6. I. Dutta, S.M. Allen, and J.L. Hafley: *Metall. Trans. A*, 1991, vol. 22A, pp. 2553-63.
7. S.R. Nutt and R.W. Carpenter: *Mater. Sci. Eng.*, 1985, vol. 75, pp. 169-77.
8. C.M. Friend and S.D. Luxton: *J. Mater. Sci.*, 1988, vol. 23, pp. 3173-80.
9. J.M. Papazian: *Metall. Trans. A*, 1988, vol. 19A, pp. 2945-53.
10. M. Vogelsang, R.J. Arsenault, and R.M. Fisher: *Metall. Trans. A*, 1986, vol. 17A, pp. 379-89.
11. R.J. Arsenault and R.M. Fisher: *Scripta Metall.*, 1983, vol. 17, pp. 67-71.
12. H.J. Dudek, A. Kleine, R. Borath, and G. Netie: *Mater. Sci. Eng.*, 1993, vol. A167, pp. 129-37.
13. R.J. Delasi and P.N. Adler: *Metall. Trans. A*, 1977, vol. 8A, pp. 1177-83.
14. J.M. Papazian: *Metall. Trans. A*, 1981, vol. 12A, pp. 269-80.
15. J.M. Papazian: *Metall. Trans. A*, 1982, vol. 13A, pp. 761-69.